3D laser-written silica glass step-index high-contrast waveguides for the 3.5 μm mid-infrared range

JAVIER MARTÍNEZ,[1] AIRÁN RÓDENAS,[1,*] TONEY FERNANDEZ,[2,§] JAVIER R. VÁZQUEZ DE ALDANA,[3] ROBERT R. THOMSON,[4] MAGDALENA AGUILÓ,[1] AJOY K. KAR,[4] JAVIER SOLIS,[2] AND FRANCESC DÍAZ[1]

[1]*Física i Cristal•lografia de Materials (FiCMA), Departament de Química Física i Inorgànica, Universitat Rovira i Virgili, 43007 Tarragona, Spain*
[2]*Laser Processing Group, Instituto de Óptica-CSIC, Madrid 28006 Spain*
[3]*Laser Microprocessing Group, Facultad de Ciencias, Universidad de Salamanca, 37008 Salamanca, Spain*
[4]*Institute of Photonics and Quantum Sciences, Heriot-Watt University, Edinburgh EH14 4AS, United Kingdom*
**Corresponding author: arodenas@gmail.com*
[§]Presently at *Dipartimento di Fisica, Politecnico di Milano, Milano, Italy*

Received XX Month XXXX; revised XX Month, XXXX; accepted XX Month XXXX; posted XX Month XXXX (Doc. ID XXXXX); published XX Month XXXX

We report on the direct laser fabrication of step-index waveguides in fused silica substrates for operation in the 3.5 μm mid-infrared wavelength range. We demonstrate core-cladding index contrasts of 0.7%, enabling bends, low-loss coupling to commercial fluoride fibers, and propagation losses of 1.3 (6.5) dB/cm at 3.39 (3.68) μm, close to the intrinsic losses of the glass. We also report on the existence of three different laser modified SiO_2 glass volumes, their different micro-Raman spectra, and their different temperature dependent populations of color centers, tentatively clarifying the SiO_2 lattice changes which are related to the large index changes.

OCIS codes: *(130.2755) Glass waveguides; (140.3390) Laser materials processing; (220.4000) Microstructure fabrication.*

http://dx.doi.org/10.1364/OL.99.099999

The advent of intersubband cascade lasers in the mid-90s [1-3] and of interband cascade lasers (ICL) more recently [4] played a crucial role in the development of mid-IR optical instruments (from around 2.5 to 20 μm) [5]. Likewise, due to the high interest in deploying remote mid-IR sensors, a huge work has also been done in the field of fiber growth, with fluoride and chalcogenide glasses as the most widespread solid fiber materials [6-8]. Yet these glasses have mechanical and corrosion limitations which make them unsuitable for long exposure to the environment. Chalcogenide glasses have a much lower fracture stress limit than fused silica glass, are susceptible to water corrosion, have low optical damage thresholds, and typically have toxic arsenic as primary component. Fluoride glasses also share similar mechanical, water corrosion and optical damage limitations [9]. Fused silica glass on the other hand is well known to be mechanically and thermally resilient, chemically resistant to non-fluorinated acids, solvents or plasmas, and it is currently ubiquitous in many industries, from optical fibers to microfluidic systems, microelectromechanical systems (MEMS), high temperature glassware, microscope slides, or in thermonuclear reactors as long-lifetime vacuum windows capable of withstanding high neutron and gamma irradiation levels [10-12]. Fused silica glass is however also frequently thought to be "opaque" for wavelengths above around 2.5 μm, though this is not the case for high purity fused silica glass, which maintains its high transparency to around 3.5 μm wavelength. Since novel surface sensing schemes based on dielectric loaded plasmonics [13] allow for short optical path lengths, the benefits of having a robust fused silica glass chip as light loading interface for point sensing could outweigh the limitations of intrinsic absorption losses of the material. In this letter we explore the fabrication of three-dimensional (3D) waveguides (WGs) inside silica for single-mode operation around 3.5 μm wavelength, with capability for bends with radii below 15 mm, and low numerical aperture so as to provide low-loss fiber interconnects.

In order to have embedded WGs with 3D architectures capable of interconnecting fibers as well as having on-chip functional WG circuits, the 3D direct laser writing technique (DLW) has become the standard technique after almost 20 years of research, being fused silica the considerably most studied material [14-20]. Our DLW setup consisted on an fs-fibre-laser amplifier (Tangerine, Amplitude Systemes) delivering ~450 fs pulses at 1047 nm and at a rate of 500 KHz. The laser power was kept at 400 mW by means of neutral density filters and the beam was circularly polarized. The laser beam was focused inside Suprasil 300 (S300, Heraeus) high purity silica using an aspheric lens with 0.4 NA. The sample was translated at a speed of 1.5 mm/s, and the multiscan approach was used [16], with a scan separation of 0.4 μm. For this work we performed a study of WG depth fabrications down to 1480 μm, so as to evaluate the potential for inscribing "on the fly" 3D circuits. After WG fabrication the sample facets were polished to optical quality, characterized under bright-field microscopy, and characterized in a mid-IR guiding setup. Our guiding setup consisted on a 1.5 mW HeNe laser (3.39 μm) and a 3 mW ICL tunable laser (from 3.57 to 3.68 μm). Both lasers provided vertically polarized beams. A pair of lenses with NA=0.18 (Thorlabs C021TME-E) were used for in and out-coupling laser light from the WGs. A Thorlabs (PDA20H-EC) PbSe amplified detector was used in combination with a FLIR SC700 camera for imaging the output WG modes. COMSOL software was used to simulate the WGs modes assuming step-index profiles and the measured core sizes from bright-field microscopy. By changing the core refractive index the simulated mode field diameters (MFDs) could be made to match the experimentally found values, therefore obtaining

approximate inferred values for the core index changes $\Delta n = n_{core} - n_{cladding}$ for all WGs.

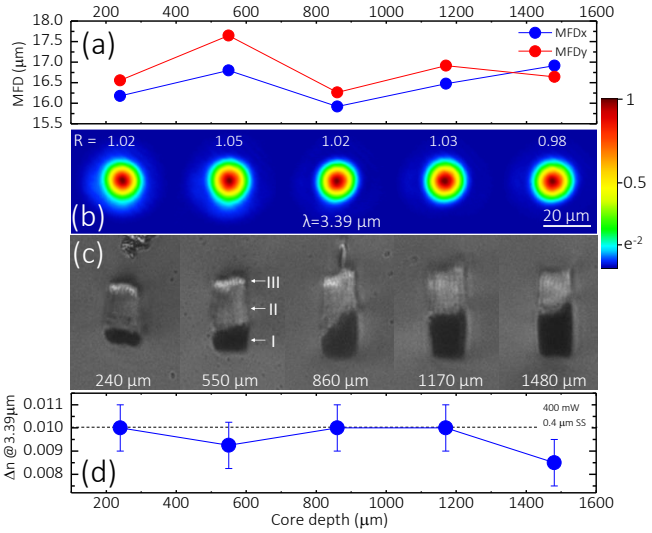

Fig. 1. Mid-IR at 3.39 μm wavelength vertically-polarized guiding characterization of WGs: (a) horizontal -x- and vertical -y- mode field diameters, (b) output near-field images, (c) bright-field transmission images of WGs, (d) inferred approximate core index changes.

Figure 1 shows a summary of the characterization results performed at 3.39 μm. Fig. 1(a) shows the measured MFDs for horizontal (x) and vertical (y) directions, and for 5 different WG depths. As it can be seen the MFDs only changed within ±1 μm for all depths. Fig. 1 (b) shows the near-field images of the 5 WGs and the MFD´s vertical to horizontal ratios (R). The mode ratios are measured to be almost constant at R=1±5%, which is fundamental for ensuring low-loss coupling to optical fibers. Fig. 1(c) shows the bright field images of the WGs at different depths. Three different zones observed in the WGs are labelled I to III. The first two zones (I and II) are well known and correspond to Type II and Type I index modifications, respectively [21, 22]. Type I modifications consist on index increased volumes and Type II regions are typically depressed index zones with a strongly anisotropic nanograting inner structure. The core waveguiding region is assumed to be zone II and perhaps also zone III. The brighter third region (III) is here reported for the first time to our knowledge, in fused silica. Finally, Fig. 1 (d) shows the corresponding estimated Δn values for different fabrication depths, which in average is of 0.01 ±0.0015.

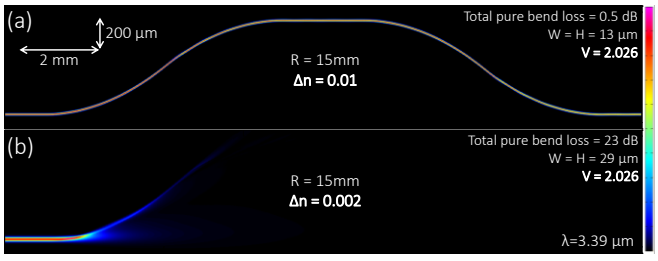

Fig. 2. Simulated intensity profiles comparison between two bent comparable WGs with high Δn = 0.01 (a), and low Δn = 0.002 (b).

The NA of these WGs $NA=(n_{core}^2-n_{dad}^2)^{1/2}$ is of NA~0.17, allowing for low loss coupling to commercial fluoride optical fibers, which also adds to the advantage of reduced Fresnel losses between fused silica and fluoride glasses. Importantly, a value of Δn=0.01 with the low cladding index of 1.4095 of silica at 3.39 μm, indicates that these WGs have a high index contrast $C\%=\Delta n/n_{core}$ of ~0.7% for DLW WGs. This contrast value at 3.39 μm is higher than previously reported values for DLW WGs in chalcogenide glass (~0.55%) [23] and borate crystals (~0.29%) [24], allowing for tighter bend radii without significant losses. It is also appropriate to indicate that the typical values of Δn for multiscan DLW WGs in silica are lower of around 2E-3 [25].

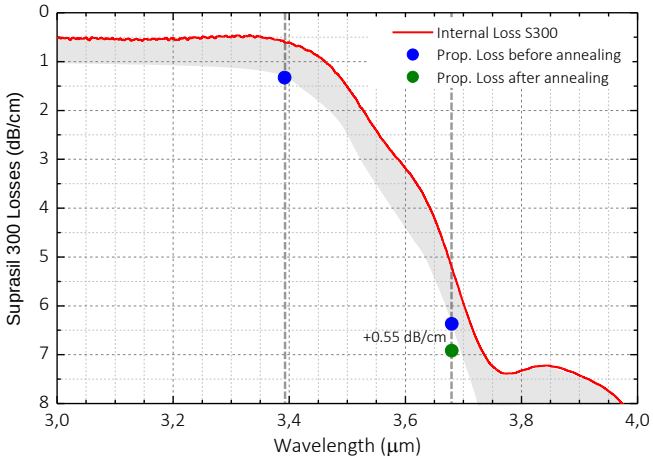

Fig. 3. Measured transmission spectrum of S300 sample together with the WG propagation loss values at different wavelengths.

The key importance of increasing the contrast with step-index WGs is depicted on **Figure 2** with a comparison of two equivalent s-bent WGs performed using the Beam Propagation Method (BPM) with the RSoft BeamPROP package. Fig. 2 (a) shows a simulation of the WGs with core sizes of ~13 μm, Δn=0.01 and a normalized frequency parameter V=2.026, which for two s-bends with radii of 15 mm yield a total radiation loss of only 0.5 dB, whereas a peer step-index WG with reduced index Δn=0.002 and same V parameter loses all the light before starting the first bend. It is also important to note that previous studies in DLW multiscan WGs in borate crystals have shown that the index increase in the modified region is wavelength dependent, as it was estimated to be the double at shorter (1.9 μm) than at longer (3.4 μm) wavelengths [23]. This indicates that the fabricated WGs could have increased Δn values at the near-IR or visible range.

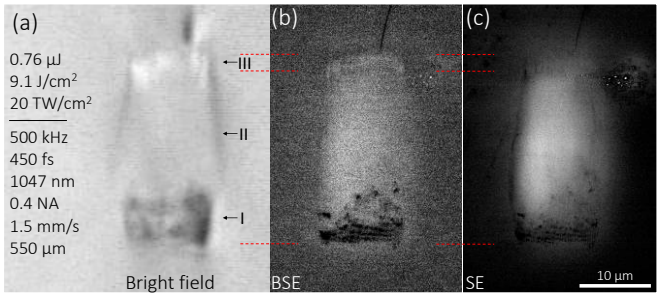

Fig. 4. Optical bright-field (a), back-scattered electrons (b), and secondary electrons (c) images of a WG. Volumes I, II, and III indicated.

The insertion losses (IL) were measured for all the WGs. The coupling losses (CL) were estimated using the overlap integral between the measured WG mode and the measured focal spot of the input/output lenses. The propagation losses (PL) were then obtained from PL=(IL–2 CL)/L, where L is the WG length. **Figure 3** shows the measured transmission spectrum of the S300 sample and the WG PLs at 550 μm depth. The PLs follow closely the transmission of S300, being of 1.3 (6.5) dB/cm at 3.39 (3.68) μm wavelength. In order to evaluate the thermal resistance of the WGs, the sample was also submitted to a two-step annealing process: a first annealing step for 2h at 200˚C and a second one at 400˚C were performed. After the annealing the WGs were almost unmodified and only the PL at 3.68 μm was observed to slightly deteriorate by +0.55 dB/cm (see Fig. 3).

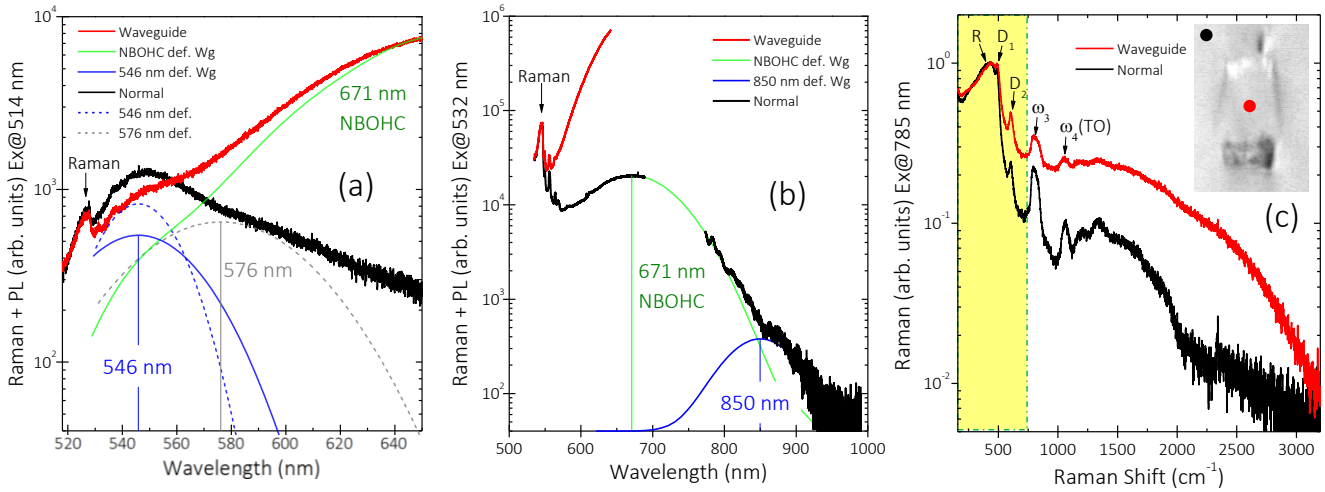

Fig. 5. Micro-Raman spectra inside and outside of the WG: (a) excitation at 514 nm yields a dominant emission of 3 color centers, (b) excitation at 532 nm yields Raman and emission from NBOHCs, (c) excitation at 785 nm yields clear Raman with no luminescence background. All graphs are in logarithmic scale for clarity of all spectral features.

The fact the WG PLs are 0.5 dB larger than the glass intrinsic absorption at 3.39 μm, and even 1.0 dB larger at the longer wavelength of 3.68 μm, suggests that a larger mode would have a further extension in the nanograting zone I, where light scattering is likely to happen. To better understand the morphology of the multiscan WGs a detailed analysis of the WGs was performed. **Figure 4** shows optical bright-field, back-scattered electrons (BSE), and secondary electrons (SE) micrographs of the WG output facet. These images allow to better differentiate volume I (nanogratings regions), II (index increased core), and III. The BSE image clearly shows that the core region (II) and region III correspond to densified SiO_2 glass.

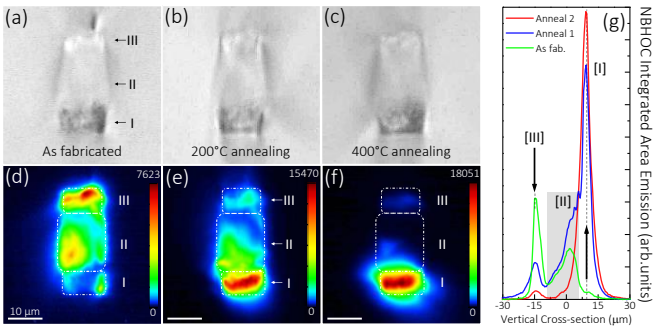

Fig. 6. Micro-mapping of NBOHCs. (a, d) As fabricated WG, (b, e) after 200˚C first annealing, (c, f) 400˚C second annealing, (g) compared vertical cross-sections of the 3 maps.

Further information on these micro-modifications can be obtained from micro-spectroscopy mapping of the WG facet. With this aim we first performed micro-Raman confocal measurements both in the center of the WG core (zone II) as in unmodified glass volume (see Ref. [23] for further experimental setup details). **Figure 5** shows the Raman and luminescence spectra obtained at three different excitation wavelengths. Gaussian fits were used to deconvolute the different broad emission bands of luminescent centers. Excitation at 514 nm in unmodified S300 produces broad emission of oxygen deficiency centers (ODCs) with peak intensity at 546 nm (2.27 eV), as well as of an unknown laser induced defect (LID) at 576 nm (2.15 eV) [22]. At the WG core however, strong emission from non-bridging oxygen-hole centers (NBOHCs) is also observed. When exciting at 532 nm only NBOHCs are observed to emit both from unmodified S300 glass and from the WG core, although the emission peak intensity coming from the core is almost 20-fold more intense. Lastly, when exciting at 785 nm no color center is excited and the Raman spectrum is accurately measured (Fig.5 (c)). **Figure 6** further presents a summary of the NBOHC emission mapping of the WG cross-section before and after the annealing process, revealing that in the as-fabricated WG the highest concentration of NBOHCs is located at region III, but after thermal annealing NBOHCs are remarkably activated at region I (nanogratings) and almost erased from other volumes. This confirms that the origin of the step Δn at the WG core (zone II) is not originated by NBOHCs but from the higher density observed from brighter BSEs (see Fig. 4(b)).

A micro-Raman map (**Figure 7**) was also performed in the WG, before and after annealings, in order to evaluate the lattice changes produced at each modified volume. Results were very similar in both cases so after-annealing results are not shown for the sake of brevity. Fig. 7(k) shows representative spectra at: unmodified S300 glass, top of the core (region III), core (region II), and at the bottom (nanogratings) region I. The integrated area map of the broad R phonon band (Fig. 7 (b)) shows a decrease of 26% from normal to zone I, indicating that at zone I (nanogratings) indeed bond breaking occurs. Moreover, a phonon at 707 cm^{-1} with narrow crystal-like FWHM of only 13.5 cm^{-1} is detected at zone I only (Fig. 7 (d)) (and which disappeared after 400˚C annealing), indicating that fundamental structural transformations of the SiO_2 glass structure occur at this nanostructured volume. This phonon has never been reported in SiO_2 glass to our knowledge, and we tentatively assign it to the identified A_g mode at 705 cm^{-1} from Si-O-Si characteristic bending vibrations of ordered SiO_2 polyhedra in Jadeite [27]. Fig. (e) to (j) show the maps of phonon energy, FWHM and area of D_1 and D_2 rings. At region III higher phonon energies for both D_1 and D_2 are observed, indicating a probable higher compaction level of these ring defects, compared to region II. Finally, we also analyzed the ratio of integrated areas of D_1 and D_2 rings, finding a clear trend in which the depressed index zone I has a high ratio value of ~3, while positive Δn zones II and III show a much lower value of ~1.85 down to ~1.1. The use of this ratio coefficient could prove useful as indicator of refractive index increased areas in DLW fused silica glass.

In conclusion, we have demonstrated the 3D DLW of step-index WGs in SiO_2 glass capable of guiding at around 3.5 μm range. We have proved these WGs can sustain temperatures of up to 400˚C, and can provide low-loss coupling to mid-IR fluoride fibers. We have also studied the microstructural changes associated with the femtosecond pulse laser modified glass, identifying three different states of SiO_2 glass state.

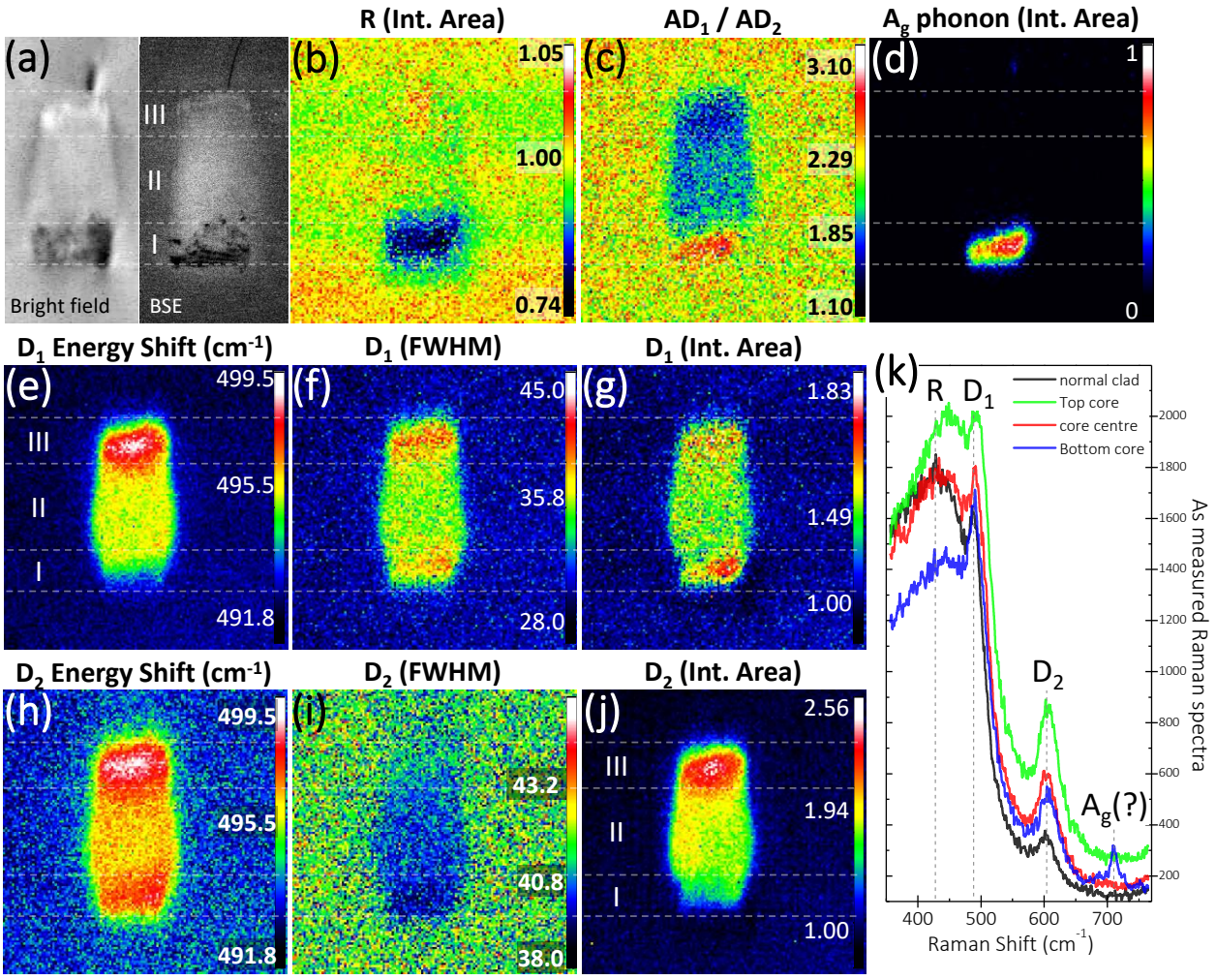

Fig. 7. Raman characterization of WG: (a) bright-field and BSE images, (b) integrated area of R mode, (c) ratio of the areas of D_1 and D_2 defect modes, (d) area of the 707 cm^{-1} (A_g) mode, (e) and (h) energy shifts of D_1 and D_2, (f) and (i) FWHM of D_1 and D_2, (g) and (j) areas of the D_1 and D_2, and (k) representative Raman spectra at non-modified normal point and at each of the 3 modified zones.

Funding. Spanish Government (MAT2013-47395-C4-4-R, TEC2014-55948-R, TEC2014-52642-C2-1-R, and FIS2013-44174-P). Catalan Government (2009SGR235 and 2014FI_B 00274). European Commission (ACP2-GA-2013-314335-JEDI ACE).

REFERENCES

1. J. Faist, F. Capasso, D. L. Sivco, C. Sirtori, A. L. Hutchinson, and A. Y. Cho, Science 264, 5158 (1994)
2. Y. Yao, A. J. Hoffman, and C. F. Gmachl, Nat. Photon **6**, 432 (2012)
3. M. S. Vitiello, G. Scalari, B. Williams, and P. De Natale, Opt. Express **23**, 5167 (2015)
4. W. Zeller, L. Naehle, P. Fuchs, F. Gerschuetz, L. Hildebrandt, and J. Koeth, *DFB Lasers Between 760 nm and 16 µm for Sensing Applications*. Sensors 10, 2492 (2010)
5. C. R. Webster, P. R. Mahaffy, S. K. Atreya, G. J. Flesch, K. A. Farley, and the MSL Science Team, Science **342**, 355 (2013)
6. M. Saad, Proc. SPIE 7316, Fiber Optic Sensors and Apps. VI, 73160N (2009)
7. V. Fortin, M. Bernier, S. T. Bah, and R. Vallée, Opt. Lett. **40**, 2882 (2015)
8. B. Bureau, C. Boussard-Plédel, V. Nazabal, J. Adam, and J. Lucas, in Advanced Photonics, OSA Technical Digest (online), paper SeTh1C.1. OSA 2014
9. N. Caron, M. Bernier, D. Faucher, and R. Vallée, Opt. Express **20**, 22188 (2012)
10. Y. Bellouard, A. Said, and P. Bado, Opt. Express **13**, 6635 (2005)
11. Y. Bellouard, Opt. Mater. Express **1**, 816 (2011)
12. I. I. Orlovskiy, K. Yu. Vukolov, E. N. Andreenko, and T. R. Mukhammedzyanov, J. Nucl. Mat. **442**, 1–3, Suppl. 1, 508 (2013)
13. B. Schwarz, P. Reiniger, D. Ristanic, H. Detz, A. M. Andrews, W. Schrenk, and G. Strasser, Nat. Commun. **5**, 4085 (2014)
14. K. M. Davis, K. Miura, N. Sugimoto, and K. Hirao, Opt. Lett. **21**, 1729 (1996)
15. A. Marcinkevičius, S. Juodkazis, M. Watanabe, M. Miwa, S. Matsuo, H. Misawa, and J. Nishii, Opt. Lett. **26**, 277 (2001)
16. Y. Nasu, M. Kohtoku, and Y. Hibino, Opt. Lett. **30**, 723 (2005)
17. G. D. Marshall, M. Ams, and M. J. Withford, Opt. Lett. **31**, 2690 (2006)
18. R. R. Thomson, H. T. Bookey, N. D. Psaila, A. Fender, S. Campbell, W. N. MacPherson, J. S. Barton, D. T. Reid, and A. K. Kar, Opt. Express **15**, 11691 (2007)
19. S. J. Beecher, R. R. Thomson, B. P. Pal and A. K. Kar, Sensors Journal, IEEE **12**, 5, 1263 (2012)
20. G. Cheng, C. D'Amico, X. Liu, and R. Stoian, Opt. Lett. **38**, 1924 (2013)
21. Y. Shimotsuma, P. G. Kazansky, J. Qiu, and K. Hirao, Phys. Rev. Lett. **91**, 247405 (2003)
22. R. Stoian, K. Mishchik, G. Cheng, C. Mauclair, C. D'Amico, J. P. Colombier, and M. Zamfirescu, Opt. Mater. Express **3**, 1755 (2013)
23. A. Ródenas, G. Martin, B. Arezki, N. Psaila, G. Jose, A. Jha, L. Labadie, P. Kern, A. Kar, and R. Thomson, Opt. Lett. **37**, 392 (2012)
24. A. Rodenas and A. K. Kar, Opt. Express **19**, 17820 (2011)
25. W. Watanabe, Y. Note, and K. Itoh, Opt. Lett. **30**, 2888 (2005)
26. S. M. Eaton, M. L. Ng, R. Osellame, and P. R. Herman, J. Non-Cryst. Solids **357** (11-13), 2387 (2011)
27. M. Prencipe, J. Raman Spectrosc. **43**, 1567 (2012)

REFERENCES FOR REVIEWING:

1. J. Faist, F. Capasso, D. L. Sivco, C. Sirtori, A. L. Hutchinson, and A. Y. Cho, "*Quantum Cascade Laser*", Science 264, 5158 (1994)
2. Y. Yao, A. J. Hoffman, and C. F. Gmachl, "*Mid-infrared quantum cascade lasers*", Nat. Photon **6**, 432 (2012)
3. M. S. Vitiello, G. Scalari, B. Williams, and P. De Natale, "*Quantum cascade lasers: 20 years of challenges*", Opt. Express **23**, 5167 (2015)
4. W. Zeller, L. Naehle, P. Fuchs, F. Gerschuetz, L. Hildebrandt, and J. Koeth, "*DFB Lasers Between 760 nm and 16 µm for Sensing Applications*". Sensors 10, 2492 (2010)
5. C. R. Webster, P. R. Mahaffy, S. K. Atreya, G. J. Flesch, K. A. Farley, and the MSL Science Team, "*Low Upper Limit to Methane Abundance on Mars*", Science **342**, 355 (2013)
6. M. Saad, "*Fluoride glass fiber: state of the art*", Proc. SPIE 7316, Fiber Optic Sensors and Applications VI, 73160N (2009)
7. V. Fortin, M. Bernier, S. T. Bah, and R. Vallée, "*30 W fluoride glass all-fiber laser at 2.94 µm*", Opt. Lett. **40**, 2882 (2015)
8. B. Bureau, C. Boussard-Plédel, V. Nazabal, J. Adam, and J. Lucas, "*Chalcogenide optical fibers for mid-infrared sensing: state of the art and future strategies*", in Advanced Photonics, OSA Technical Digest (online), paper SeTh1C.1. OSA 2014
9. N. Caron, M. Bernier, D. Faucher, and R. Vallée, "*Understanding the fiber tip thermal runaway present in 3µm fluoride glass fiber lasers*", Opt. Express **20**, 22188 (2012)
10. Y. Bellouard, A. Said, and P. Bado, "*Integrating optics and micro-mechanics in a single substrate: a step toward monolithic integration in fused silica*", Opt. Express **13**, 6635 (2005)
11. Y. Bellouard, "*On the bending strength of fused silica flexures fabricated by ultrafast lasers*", Opt. Mater. Express **1**, 816 (2011)
12. I.I. Orlovskiy, K.Yu. Vukolov, E.N. Andreenko, T.R. Mukhammedzyanov, "*Neutron irradiation of modern KU-1 and KS-4V fused silica*", Journal of Nuclear Materials, **442**, 1–3, Supplement 1, 508 (2013)
13. B. Schwarz, P. Reiniger, D. Ristanic, H. Detz, A. M. Andrews, W. Schrenk, and G. Strasser, "*Monolithically integrated mid-infrared lab-on-a-chip using plasmonics and quantum cascade structures*", Nat. Commun. **5**, 4085 (2014)
14. K. M. Davis, K. Miura, N. Sugimoto, and K. Hirao, "*Writing waveguides in glass with a femtosecond laser*", Opt. Lett. **21**, 1729 (1996)
15. A. Marcinkevičius, S. Juodkazis, M. Watanabe, M. Miwa, S. Matsuo, H. Misawa, and J. Nishii, "*Femtosecond laser-assisted three-dimensional microfabrication in silica*," Opt. Lett. **26**, 277 (2001)
16. Y. Nasu, M. Kohtoku, and Y. Hibino, "*Low-loss waveguides written with a femtosecond laser for flexible interconnection in a planar light-wave circuit*," Opt. Lett. **30**, 723 (2005)
17. G. D. Marshall, M. Ams, and M. J. Withford, "*Direct laser written waveguide-Bragg gratings in bulk fused silica*," Opt. Lett. **31**, 2690 (2006)
18. R. R. Thomson, H. T. Bookey, N. D. Psaila, A. Fender, S. Campbell, W. N. MacPherson, J. S. Barton, D. T. Reid, and A. K. Kar, "*Ultrafast-laser inscription of a three dimensional fan-out device for multicore fiber coupling applications*," Opt. Express **15**, 11691 (2007)
19. S. J. Beecher, R. R. Thomson, B. P. Pal and A. K. Kar, "*Single Stage Ultrafast Laser Inscription of a Side-Polished Fiber-Like Waveguide Sensor*," Sensors Journal, IEEE **12**, 5, 1263 (2012)
20. G. Cheng, C. D'Amico, X. Liu, and R. Stoian, "*Large mode area waveguides with polarization functions by volume ultrafast laser photoinscription of fused silica*," Opt. Lett. **38**, 1924 (2013)
21. Y. Shimotsuma, P. G. Kazansky, J. Qiu, and K. Hirao, "*Self-Organized Nanogratings in Glass Irradiated by Ultrashort Light Pulses*", Phys. Rev. Lett. **91**, 247405 (2003)
22. R. Stoian, K. Mishchik, G. Cheng, C. Mauclair, C. D'Amico, J. P. Colombier, and M. Zamfirescu, "*Investigation and control of ultrafast laser-induced isotropic and anisotropic nanoscale-modulated index patterns in bulk fused silica,*" Opt. Mater. Express **3**, 1755 (2013)
23. A. Ródenas, G. Martin, B. Arezki, N. Psaila, G. Jose, A. Jha, L. Labadie, P. Kern, A. Kar, and R. Thomson, "*Three-dimensional mid-infrared photonic circuits in chalcogenide glass*," Opt. Lett. **37**, 392 (2012)
24. A. Rodenas and A. K. Kar, "*High-contrast step-index waveguides in borate nonlinear laser crystals by 3D laser writing*," Opt. Express **19**, 17820 (2011)
25. W. Watanabe, Y. Note, and K. Itoh, "*Fabrication of multimode interference waveguides in glass by use of a femtosecond laser*," Opt. Lett. **30**, 2888 (2005)
26. S. M. Eaton, M. L. Ng, R. Osellame, and P. R. Herman, "*High refractive index contrast in fused silica waveguides by tightly focused, high-repetition rate femtosecond laser*," J. Non-Cryst. Solids **357** (11-13), 2387 (2011)
27. M. Prencipe, "*Simulation of Vibrational Spectra of Crystals by Ab Initio Calculations: an Invaluable Aid in the Assignment and Interpretation of the Raman Signals. The Case of Jadeite (NaAlSi2O6)*", J. Raman Spectrosc. **43**, 1567 (2012)